DOI: 10.1002/ejic.201100095

# A Series of $Mn^{III}_4Mn^{II}_8$ Single-Molecule Magnets Mediated by Intra- and Intermolecular Interactions

**Ji-Dong Leng,[a] Long-Yang Dian,[a] Jun-Liang Liu,[a] and Ming-Liang Tong*[a]**

**Keywords:** Manganese / Tripodal ligands / Molecular interactions / Magnetic properties / Single-molecule magnets

The solvothermal reaction of manganese(II) acetylacetonate [$Mn(acac)_2$], 1,1,1-tris(hydroxymethyl)ethane ($H_3$thme), 1,1,1-tris(hydroxymethyl)propane ($H_3$thmp), and $(CH_3)_3CCO_2H$ leads to a series of mixed-valence $Mn^{III}_4Mn^{II}_8$ clusters, $[Mn^{III}_4Mn^{II}_8(\mu_5\text{-}O)_2(\mu_3\text{-}OMe)_2(thme)_4(Me_3CCO_2)_{10}(H_2O)_2]$ (**1**), $[Mn^{III}_4Mn^{II}_8(\mu_5\text{-}O)_2(\mu_3\text{-}OMe)_2(thme)_4(Me_3CCO_2)_{10}(MeOH)_2]$ (**2**), $[Mn^{III}_4Mn^{II}_8(\mu_5\text{-}O)_2(\mu_3\text{-}OMe)_2(thmp)_4(Me_3CCO_2)_{10}(H_2O)_2]$ (**3**), and $[Mn^{III}_4Mn^{II}_8(\mu_5\text{-}O)_2(\mu_3\text{-}OMe)_2(thmp)_4(Me_3CCO_2)_{10}(MeOH)_2]$ (**4**). The $Mn^{III}_4Mn^{II}_8$ cores of the complexes can be described as a central rhomboid $[Mn_4O_6]$ layer sandwiched by two $[Mn_4O_7]$ layers. Alternating current (AC) magnetization studies reveal that complexes **1**–**4** possess the $S = 4$ spin ground state and behave as single-molecule magnets (SMMs). All four of the compounds clearly show slow magnetic relaxation behavior, but out-of-phase AC peaks above 1.8 K were only obtained for **3** and **4**, thereby revealing that the ground-state anisotropy of four $Mn_{12}$ clusters are effectively modified by intra- and intermolecular interactions by substituting the tripodal ligands and terminal ligands.

## Introduction

Single-molecule magnets (SMMs) have attracted much interest in recent years[1] because they not only exhibit the properties of classical bulk magnets, but also fascinating quantum-mechanical properties, such as quantum tunneling of the magnetization vector (QTM) through the barrier.[2] Polynuclear Mn clusters, especially the clusters with the metal in the oxidation state range of II–IV and carboxylate ligands, have proven to be a fertile source of such a class of molecular materials.[1d,3,4] The necessary ingredients for a SMM to possess a significant energy barrier is large ground-state spin ($S$) and significant magnetoanisotropy of the Ising (easy-axis) type, as reflected by a negative axial zero-field splitting parameter, $D$. The upper limit of the energy barrier is given by $S^2|D|$ or $(S^{2-}¼)|D|$ for integer and half-integer $S$ values, respectively.[5] Moreover, quantum-tunneling magnetization is governed by a small transverse anisotropy term ($E$). The increase of $S$ is clearly based on ferromagnetic interactions between the spins,[1,6] whereas the enhancement of $D$ is mainly associated with the magnetic anisotropy of the cluster, which in turn depends on the local anisotropies of the single ions and their vectorial addition to give a resulting anisotropy.[1,6] However, the intermolecular interactions in the crystals can also mediate the magnetic behavior.[7]

Tripodal ligands such as 1,1,1-tris(hydroxymethyl)ethane ($H_3$thme) and 1,1,1-tris(hydroxymethyl)propane ($H_3$thmp) have been used extensively in the synthesis of oxido-vanadium and oxido-molybdenum clusters,[8] and paramagnetic 3D transition-metal clusters.[9] In particular, the use of tripodal ligands combined with flexible carboxylates in Mn chemistry has produced various products, including $\{Mn_2\}$,[4a] $\{Mn_3\}$,[4b] $\{Mn_4\}$,[4c] $\{Mn_7\}$,[4d] $\{Mn_8\}$,[4e] $\{Mn_9\}$,[4f] $\{Mn_{12}\}$,[4d,4e,4g,4h] and $\{Mn_{22}\}$[4i] SMMs. In these compounds, tripodal ligands are fully deprotonated; the arms act as a $\mu_2$ or $\mu_3$ bridge. The disposition of the three alkoxide arms of the tri-anion directs the formation of triangular $Mn_3$ units in which each arm of the ligand bridges one edge of the triangle. The combination of $Mn_3$ units and other peripheral Mn atoms bridged with these units by carboxylates or alcohols then forms the cores. Such clusters that contain many triangular building blocks or units have a great chance of displaying high or at least nonzero-spin ground states due to the presence of the large number of competing antiferromagnetic exchange interactions.[4c] It is noteworthy that all of the compounds mentioned were synthesized by room-temperature solution reactions.

We have investigated the reactions of $Mn^{II}$ acetylacetonate salts with a range of carboxylate anions and tripodal ligands in a solvothermal method to explore new routes to Mn clusters that might show SMM behavior. Herein, we present a systematic investigation on the synthesis and magnetic properties of four mixed-valence Mn clusters, $[Mn^{III}_4Mn^{II}_8(\mu_5\text{-}O)_2(\mu_3\text{-}OMe)_2(thme)_4(Me_3CCO_2)_{10}(H_2O)_2]$ (**1**),

[a] Key Laboratory of Bioinorganic and Synthetic Chemistry of Ministry of Education, State Key Laboratory of Optoelectronic Materials and Technologies, School of Chemistry and Chemical Engineering, Sun Yat-Sen University,
Guangzhou 510275, P. R. China
Fax: +86-20-8411-2245
E-mail: tongml@mail.sysu.edu.cn

Supporting information for this article is available on the WWW under http://dx.doi.org/10.1002/ejic.201100095.

  

$[Mn^{III}_4Mn^{II}_8(\mu_5\text{-}O)_2(\mu_3\text{-}OMe)_2(thme)_4(Me_3CCO_2)_{10}(MeOH)_2]$ (**2**), $[Mn^{III}_4Mn^{II}_8(\mu_5\text{-}O)_2(\mu_3\text{-}OMe)_2(thmp)_4(Me_3CCO_2)_{10}(H_2O)_2]$ (**3**), and $[Mn^{III}_4Mn^{II}_8(\mu_5\text{-}O)_2(\mu_3\text{-}OMe)_2(thmp)_4(Me_3CCO_2)_{10}(MeOH)_2]$ (**4**). The core structure of these four compounds can be described as a central rhomboid $[Mn_4O_6]$ layer sandwiched by two $[Mn_4O_7]$ layers. It should be noted that a closely related complex $[Mn_{12}O_2(OMe)_2(thme)_4(OAc)_{10}(H_2O)_4]$ similar to complexes **1**–**4** was reported by Powell's group in 2006.[4g] However, no further systematic investigation on this $Mn_{12}$ cluster family has been carried out. In our case, by substituting the mixed solvent MeOH/MeCN for **1** with pure MeOH, **2** was obtained, whereas by substituting the tripodal ligands $thme^{3-}$ in **1** and **2** with $thmp^{3-}$, **3** and **4** were obtained. These substitutions led to different coordinate modes of the pivalate ligands of the $Mn_{12}$ clusters, and the intermolecular interaction was minimized from significant hydrogen bonding in **1** and **3** to the pure van der Waals in **2** and **4**. More significantly, the ground-state anisotropies of the four $Mn_{12}$ clusters are then effectively modified.

## Results and Discussion

### Synthesis

Most of the mixed-valence manganese clusters were synthesized by means of a conventional manganese redox reaction ($MnO_4^-$ oxidizing $Mn^{2+}$) or room-temperature solution reactions of manganese(II) salts. This series of $Mn^{III}_4Mn^{II}_8$ clusters was synthesized by the solvothermal reactions of $Mn^{II}$ acetylacetonate salts with pivalic acid and tripodal ligands, which have rarely been used to prepare discrete molecular clusters other than the polyoxovanadates and -molybdates.[10] Superheated solvents exhibit (1) reduced viscosity (and therefore enhanced diffusion of chemical species) and (2) very different solubilizing properties (e.g., the dielectric constant of water decreases rapidly with increasing temperature)[11] compared to ambient conditions. Note that the vessel was not full of solvent; the four $Mn^{III}$ ions in the molecule might be oxidized by the air in the vessel from $Mn^{II}$ acetylacetonate. As a result of an unknown brown precipitate being obtained with the crystal, the yield of **1**–**4** is not very high (30–50%).

### Description of Structures

The structures of the complete $Mn_{12}$ molecules of **1**–**4** are shown in Figures 1, 2, 3, and 4, respectively. Selected interatomic distances and angles are listed in Tables S1 and S2 in the Supporting Information, respectively.

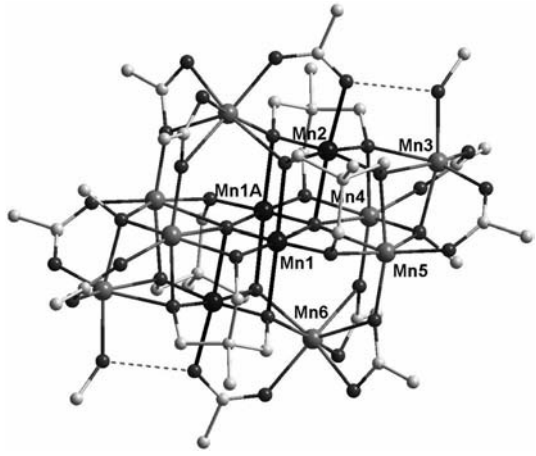


Figure 2. Structure of the complete $Mn_{12}$ molecule of **2** with intramolecular hydrogen bonds shown as dashed lines. Hydrogen atoms and pivalate Me groups have been omitted for clarity. The thicker black bonds indicate the $Mn^{III}$ Jahn–Teller elongation axes. Symmetry code: A: $-x + 1, -y, -z$.

Complex **1** crystallizes in the triclinic space group $P\bar{1}$ with the $Mn_{12}$ cluster lying on an inversion center. The complex contains a $[Mn_{12}(\mu_5\text{-}O)_2(\mu_3\text{-}O)_{10}(\mu_2\text{-}O)_8]$ core (Figure 1b), which can be described as a central rhomboid $[Mn_4O_6]$ layer (Mn1, Mn2, O1, O5, O6, and their symmetry

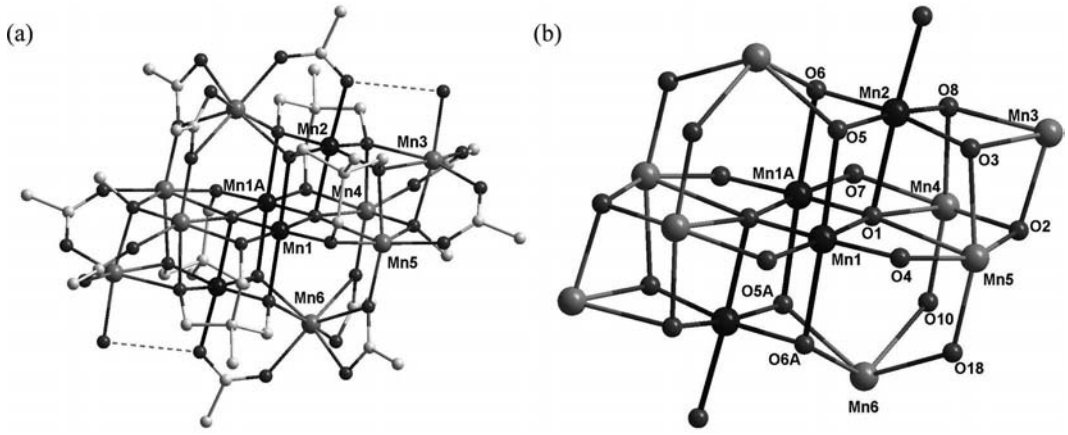


Figure 1. (a) Structure of the complete $Mn_{12}$ molecule of **1** with intramolecular hydrogen bonds shown as dashed lines. Hydrogen atoms and pivalate Me groups have been omitted for clarity. The thicker black bonds indicate the $Mn^{III}$ Jahn–Teller elongation axes. (b) Central core of **1**. Symmetry code: A: $-x + 1, -y + 1, -z$.

  

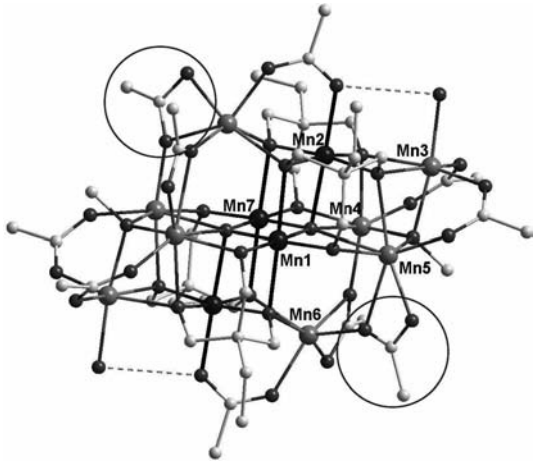


Figure 3. Structure of the complete $Mn_{12}$ molecule of **3** with intramolecular hydrogen bonds shown as dashed lines. Hydrogen atoms and pivalate Me groups have been omitted for clarity. The thicker black bonds indicate the $Mn^{III}$ Jahn–Teller elongation axes. Symmetry code: A: $–x + 3/2, –y + 3/2, z$.

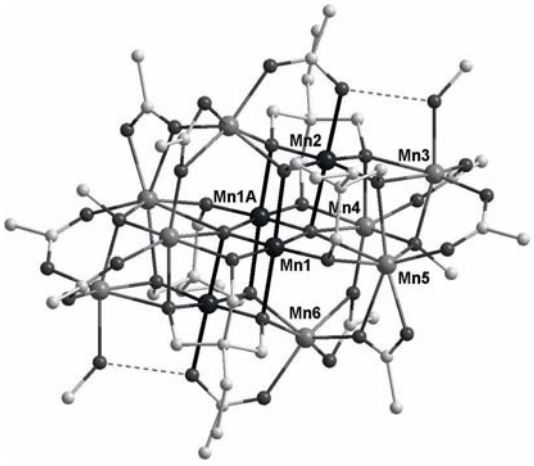


Figure 4. Structure of the complete $Mn_{12}$ molecule of **4** with intramolecular hydrogen bonds shown as dashed lines. Hydrogen atoms and pivalate Me groups have been omitted for clarity. The thicker black bonds indicate the $Mn^{III}$ Jahn–Teller elongation axes. Symmetry code: A: $–x, –y + 2, –z$.

equivalents) sandwiched by two $[Mn_4O_7]$ layers (Mn3, Mn4, Mn5, Mn6, O2, O3, O4, O7, O8, O12, O18, and their symmetry equivalents). The structure of this core is reminiscent of the rock-salt lattice type, except for Mn6, which was pulled out of position by the chelating acetates. With the exception of Mn6, which is seven-coordinate, all of the Mn ions are six-coordinate with distorted octahedral geometry. Charge-balance consideration and the presence of $Mn^{III}$ Jahn–Teller (JT) distortions (axial elongations on Mn1 and Mn2) indicate an $Mn^{II}_8Mn^{III}_4$ description, as confirmed by bond-valence sum (BVS) calculations (Table 1).[12] Notably, the Mn ions in the central and the side layers are $Mn^{III}$ and $Mn^{II}$, respectively, to form a valence-sandwich-type topology, which has rarely been reported in Mn clusters.[13] All of the elongation axes of the four $Mn^{III}$ centers are close to co-parallel. This alignment will dominate the magnetic anisotropy (i.e., the magnitude of the ZFS parameter, *D*) of the complete $Mn_{12}$ molecule, which will be of relevance to the discussion of the magnetic properties later.

Table 1. BVS for the Mn atoms in **1**–**4**[a].

| Atom | $Mn^{II}$ | $Mn^{III}$ | $Mn^{IV}$ | Atom | $Mn^{II}$ | $Mn^{III}$ | $Mn^{IV}$ |
|---|---|---|---|---|---|---|---|
| **1** | | | | **3** | | | |
| Mn1 | 3.27 | ***3.02*** | 2.54 | Mn1 | 3.36 | ***3.10*** | 3.04 |
| Mn2 | 3.40 | ***3.14*** | 3.08 | Mn2 | 3.46 | ***3.19*** | 3.13 |
| Mn3 | ***1.96*** | 1.81 | 1.78 | Mn3 | ***2.01*** | 1.86 | 1.82 |
| Mn4 | ***2.16*** | 1.99 | 1.82 | Mn4 | ***2.11*** | 1.95 | 1.73 |
| Mn5 | ***2.11*** | 1.83 | 1.80 | Mn5 | ***2.03*** | 1.88 | 1.56 |
| Mn6 | ***1.86*** | 1.60 | 1.18 | Mn6 | ***2.04*** | 1.88 | 1.85 |
| | | | | Mn7 | 3.35 | ***3.09*** | 3.03 |
| **2** | | | | **4** | | | |
| Mn1 | 3.23 | ***2.98*** | 2.52 | Mn1 | 3.32 | ***3.06*** | 2.80 |
| Mn2 | 3.36 | ***3.10*** | 3.04 | Mn2 | 3.40 | ***3.14*** | 3.08 |
| Mn3 | ***2.14*** | 1.98 | 1.81 | Mn3 | ***2.03*** | 1.88 | 1.63 |
| Mn4 | ***2.09*** | 1.93 | 1.89 | Mn4 | ***2.11*** | 1.94 | 1.74 |
| Mn5 | ***2.07*** | 1.79 | 1.76 | Mn5 | ***1.99*** | 1.72 | 1.53 |
| Mn6 | ***1.86*** | 1.61 | 1.22 | Mn6 | ***1.97*** | 1.81 | 1.59 |

[a] Values printed in ***bold italics*** are the closest to the charge for which it was calculated; the nearest whole number can be taken as the oxidation state of that atom.

BVS calculations were performed on the inorganic O atoms to assess their degree of protonation (Table S3 in the Supporting Information). These confirm two terminal $H_2O$ ligands and two $\mu_5$-$O^{2–}$ ions, which is rather unusual in manganese carboxylate clusters. The methoxo ligands adopt a typical $\mu_3$-bridging mode. The four $thme^{3–}$ ligands are fully deprotonated with the same type: each of them uses two arms in a $\mu_3$-fashion, whereas the third arm acts as a $\mu_2$-bridge. Peripheral ligation is provided by 10 pivalate groups that exhibit two binding modes: six bridge two Mn atoms in the common *syn*,*syn*, μ-bridging mode, another four adopt a less common chelate-bridging mode.[3d] The terminal aqua ligands form hydrogen bonds to pivalate ligands, either in the same molecule or to pivalate ligands in neighboring molecules, thus forming a linear one-dimensional chain of $Mn_{12}$ molecules along the *c* axis (Figure 5). The shortest intercluster Mn···Mn distance is 4.883 Å.

Notably, $Mn_{12}$ pivalate complex **1** is similar to a reported $Mn_{12}$ acetate complex $[Mn_{12}O_2(OMe)_2(thme)_4(OAc)_{10}(H_2O)_4]$ (**5**).[4g] The difference between **1** and **5** is evident in both the peripheral groups and the packing mode of the $Mn_{12}$ molecules: the latter contains two terminal acetate ligands and four $H_2O$ ligands to form a planar two-dimensional packing, in contrast to the absence of terminal pivalate ligands and only two $H_2O$ ligands that form a linear one-dimensional chain in complex **1** (Figure 5, a). These dissimilarities of the structure effect a significant change in their magnetic properties, which will be discussed later.

Complex **2** crystallizes in the monoclinic space group *C*2/*c* with almost the same core structure (Figure S1 in the Supporting Information) as complex **1**, except the terminal aqua ligands are replaced with MeOH. The difference between **1** and **2** is the packing mode of the $Mn_{12}$ molecules (Figure 5, b). No significant intermolecular interactions in complex **2** can be observed. As a result, the shortest inter-

  

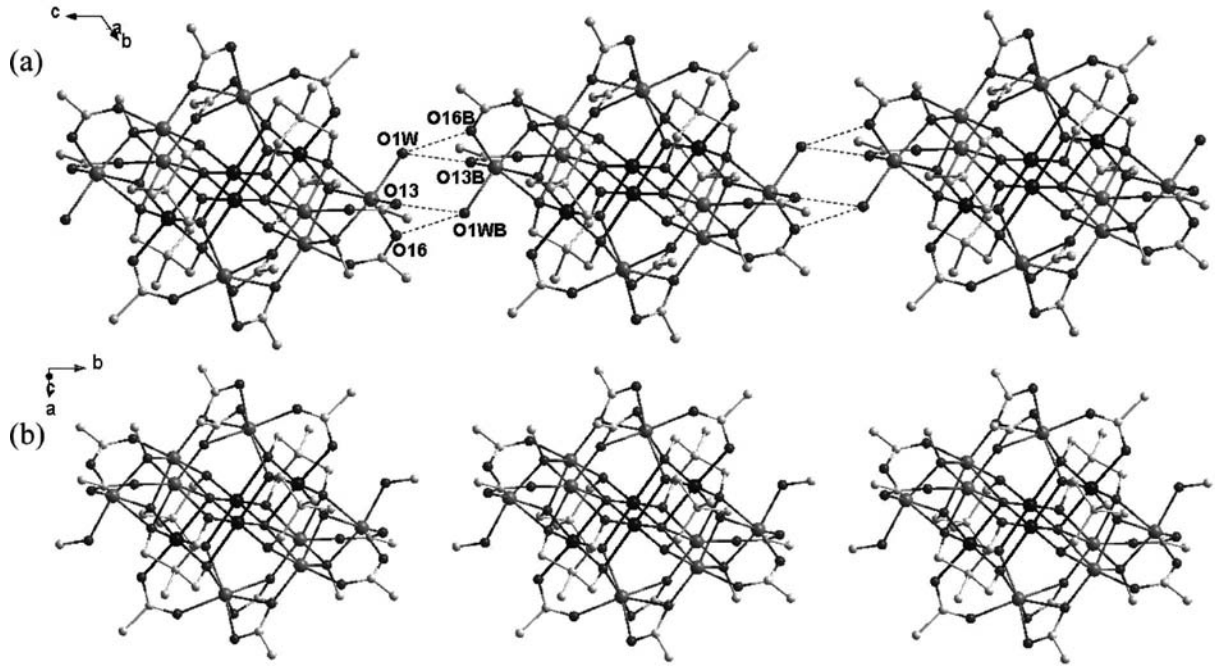


Figure 5. (a) The packing arrangement of **1** along the *c* axis. Hydrogen atoms and pivalate Me groups have been omitted for clarity. The terminal aqua ligand forms two hydrogen bonds with the pivalate groups of the neighboring molecule: O1W···O13B 3.136 Å, O1W···O16B 3.113 Å. Symmetry code: B: $-x + 1$, $y + 1$, $-z - 1$. (b) The packing arrangement of **2** along the *b* axis. Hydrogen atoms and pivalate Me groups have been omitted for clarity.

cluster Mn···Mn distance is significantly elongated from 4.883 Å in complex **1** to 6.271 Å in complex **2**. The different packing mode of these two complexes make significant changes in their intermolecular magnetic interactions.

Complex **3** crystallizes in the orthorhombic space group *Pccn* with a similar structure to **1**. Except for the fact that the thme$^{3-}$ ligands are replaced with thmp$^{3-}$, the evident difference between **3** and **1** is one of the pivalate groups,

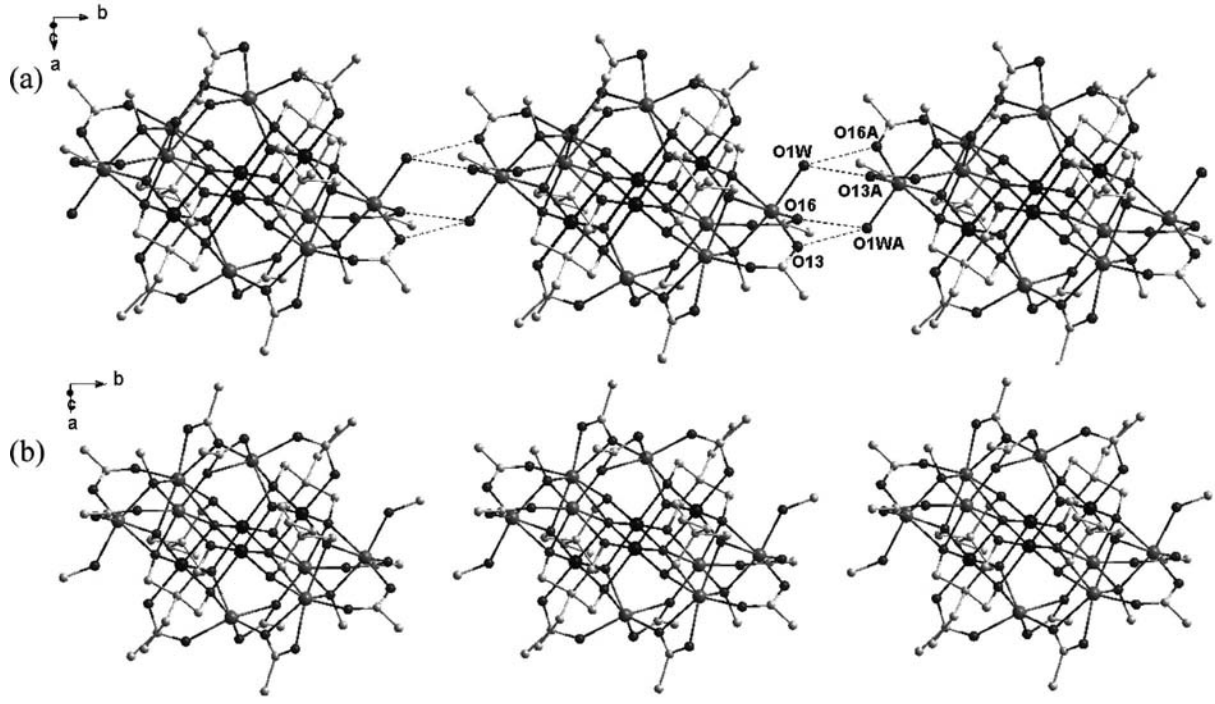


Figure 6. (a) The packing arrangement of **3** along the *b* axis. Hydrogen atoms and pivalate Me groups have been omitted for clarity. The terminal aqua ligand forms two hydrogen bonds with the pivalate groups of neighboring molecule: O1W···O13A 3.110 Å, O1W···O16A 3.178 Å. Symmetry code: A: $-x + 3/2$, $-y + 5/2$, $z$. (b) The packing arrangement of **4** along the *b* axis. Hydrogen atoms and pivalate Me groups have been omitted for clarity.

  

which is highlighted in Figure 4 (a). The pivalate forms a chelate coordinated with Mn5 by both O18 and O17, and bridges Mn5 and Mn6 by O18 in **3**. In contrast, the pivalate in **1** forms a similar bridge with O18, but the chelate coordinates with Mn6 instead of Mn5. The different coordinate modes of the pivalate create significant changes in their interatomic distances and angles (Tables S1 and S2 in the Supporting Information) and also their magnetic properties. Again, the terminal aqua ligands form hydrogen bonds to pivalate ligands, either in the same molecule or to pivalate ligands in neighboring molecules, thereby forming a linear one-dimensional chain of $Mn_{12}$ molecules along the *b* axis (Figure 6). The shortest intercluster Mn···Mn distance is 5.005 Å in **3**, being slightly longer than that in **1**, which can be attributed to the steric congestion that arises from the bulk of $thmp^{3-}$ groups.

Complex **4** crystallizes in the monoclinic space group *C*2/*c*. The overall structure of complex **4** is very similar to previously characterized complex **2**, except that the $thme^{3-}$ ligands are replaced by $thmp^{3-}$. Again, the terminal methanol ligands form intramolecular hydrogen bonds to pivalate ligands. There are no significant intermolecular interactions. As a result, the shortest intercluster Mn···Mn distance is 6.337 Å in **4**, being significantly elongated from 5.005 Å in complex **3**.

## Magnetic Properties

Variable-temperature direct current (dc) magnetic-susceptibility measurements were performed on microcrystalline powder samples of **1**–**4** in a 500 G (0.05 T) field and in the 1.8–300 K range. The obtained data are shown as a $\chi_M T$ versus $T$ plot in Figure 7. Relative magnetic parameters are summarized in Table 2. Above 100 K, the magnetic susceptibilities of **1**–**4** follow a Curie–Weiss behavior. The Curie constants ($C$) range from 46.6 to 47.1 $cm^3\,K\,mol^{-1}$, which are very close to the expected value for 4 $Mn^{III}$ and 8 $Mn^{II}$ noninteracting spins (ca. 47 $cm^3\,K\,mol^{-1}$ for $g = 2$). The negative Weiss constants ($\Theta$) indicate the presence of dominant antiferromagnetic interactions within the clusters. Room-temperature $\chi_M T$ values for **1**–**4** range from 39.56 to 39.99 $cm^3\,K\,mol^{-1}$. The values are much smaller than the mentioned expected spin-only value. This phenomenon is very common in some antiferromagnetic manganese clusters. The $\chi_M T$ values then decrease gradually to values between 9.40 and 14.24 $cm^3\,K\,mol^{-1}$ at 1.8 K. The plots do not appear to be heading to zero at 0 K, thus indicating an $S > 0$ ground state. The $\chi_M T$ values at 1.8 K of **3** and **4** are notably smaller than that of **1** and **2**. It is expected due to the larger magnetic anisotropy of the molecules of **3** and **4** (vide infra).

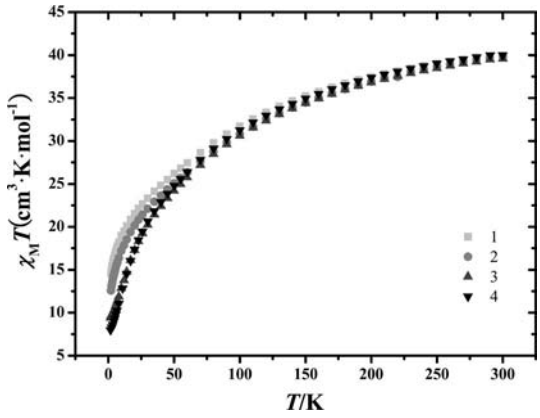


Figure 7. Plots of $\chi_M T$ versus $T$ at an applied field of 500 Oe for complexes **1**–**4**.

To determine the ground state of **1**–**4**, as well as the magnitude and sign of $D$, magnetization data were collected in a dc magnetic field and in temperature ranges of 0.05–7.0 T and 1.8–5.1 K, respectively, and were fitted by the program ANISOFIT 2.0.[14] However, attempts to fit the data collected over the whole field range were unsuccessful, which is a common problem caused by low-lying excited states, especially if some have an $S$ value greater than that of the ground state. This presumption is consistent with the isothermal field-dependent magnetizations at 1.8 K (Figure S4 in the Supporting Information), which show steadily increasing magnetization with $H$ without saturation. A common solution to get around the problem is to use only data collected at low fields, which is also regarded as a reliable method.[3d,15] But for **1** and **3**, it was still not possible to obtain a satisfactory fit. This is likely due to the intermolecular interactions mediated by the intermolecular hydrogen bonds, which cause the presence of weak exchange. Thus the likely population of excited states in the temperature range studied, and the simplistic model employed, do not allow for a reasonable fit for these data. For **2** and **4**, the best fits were carried by using the data collected at 0.05–1.0 T, with $S = 4$, $g = 1.95$, $D = -0.44\ cm^{-1}$ for **2** (Figure 8, a) and $S = 4$, $g = 2.04$, $D = -0.63\ cm^{-1}$ for **4** (Figure 8, b). The significant difference between calculated $D$ values of **2** and **4** are expected due to the varying Jahn–Teller tilts (vide infra).

Table 2. Magnetic parameters of complexes **1**–**4**.

| | $C$ [$cm^3\,mol^{-1}\,K$] | $\Theta$ [K] | $\chi_M T$ [$cm^3\,K\,mol^{-1}$] at 300 K | $\chi_M T$ [$cm^3\,K\,mol^{-1}$] at 1.8 K | $g$ | $D$ [$cm^{-1}$] | $\tau_0$ [s] | $U_{eff}$ [K] |
|---|---|---|---|---|---|---|---|---|
| **1** | 46.5 | –47.8 | 39.95 | 14.53 | n.a. | n.a. | n.a. | n.a. |
| **2** | 47.1 | –54.6 | 39.84 | 12.60 | 1.95 | –0.44 | n.a. | n.a. |
| **3** | 46.6 | –53.1 | 39.56 | 9.40 | n.a. | n.a. | $1.2\times10^{-9}$ | 30.0 |
| **4** | 47.1 | –52.1 | 39.99 | 7.99 | 2.04 | –0.63 | $1.3\times10^{-8}$ | 19.1 |

  

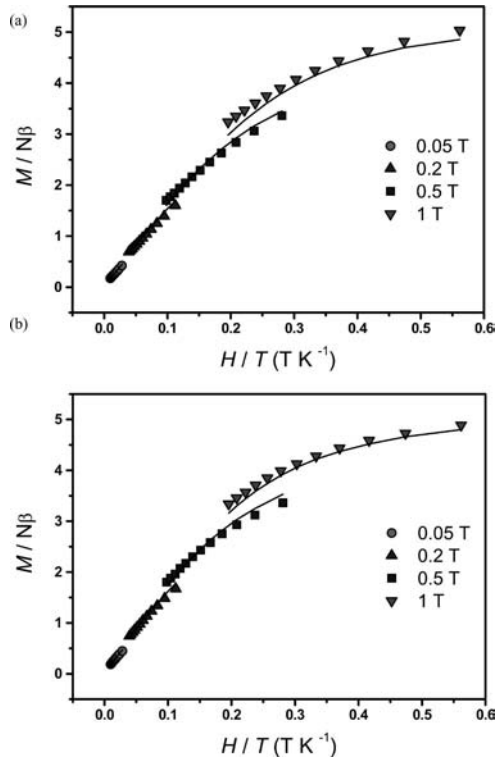


Figure 8. Plots of $M$ versus $H/T$ for (a) **2** and (b) **4** at the indicated applied fields. The solid lines are the fits of the data.

To investigate whether **1**–**4** might be SMMs, alternating current (ac) susceptibility measurements on **1**–**4** were performed in a 5 G ac field that oscillated at 1–1500 Hz and with a zero applied dc field (Figure 9). For **1** and **2**, the $\chi'_{M}T$ product (Figure 9) steadily decreases with decreasing temperature, which indicates the population of low-lying excited states with $S$ greater than the ground state $S$, thereby rationalizing the fits of dc magnetization data. Because of the absence of a dc field, ac studies could complement dc studies to get a rough estimation of the ground state of a system.[3b] Extrapolation of the plot to 0 K, at which point only the ground state will be populated, gives $\chi'_{M}T$ values of 9.74 and 11.2 cm$^3$ K mol$^{-1}$ for **1** and **2**, respectively. These two values indicate ground state $S = 4$ for both **1** and **2**. Although the $\chi'_{M}T$ versus $T$ plots show no obvious frequency dependence above 1.8 K, clearly nonzero and frequency-dependent out-of-phase ($\chi''_{M}$) ac signals were observed below 3 K (Figure 9), thus indicating a slow relaxation of the magnetization.

The ac susceptibility measurements of **3** and **4** show significantly different plots to **1** and **2**. For **3** and **4**, there are frequency-dependent decreases in $\chi'_{M}T$ and concomitant increases in $\chi''_{M}$, thus indicating **3** and **4** to be SMMs. Again, the $\chi'_{M}T$ product (Figure 10) steadily decreases with decreasing temperature, which indicates the population of low-lying excited states with $S$ greater than the ground state $S$. Extrapolation of the plot to 0 K gives a $\chi'_{M}T$ value of

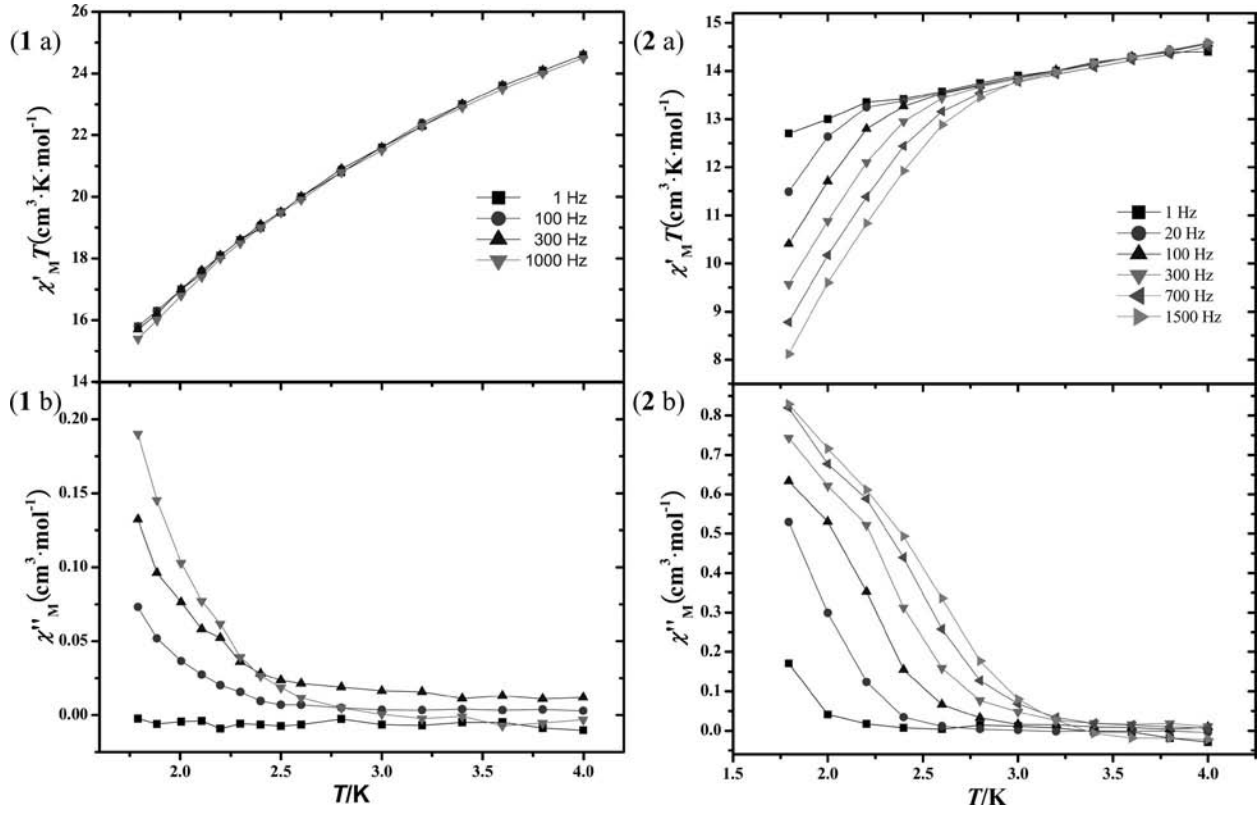


Figure 9. Temperature dependence of the in-phase (**1**a and **2**a for **1** and **2**, respectively) and out-of-phase (**1**b and **2**b for **1** and **2**, respectively) ac susceptibility at the indicated frequencies.

  

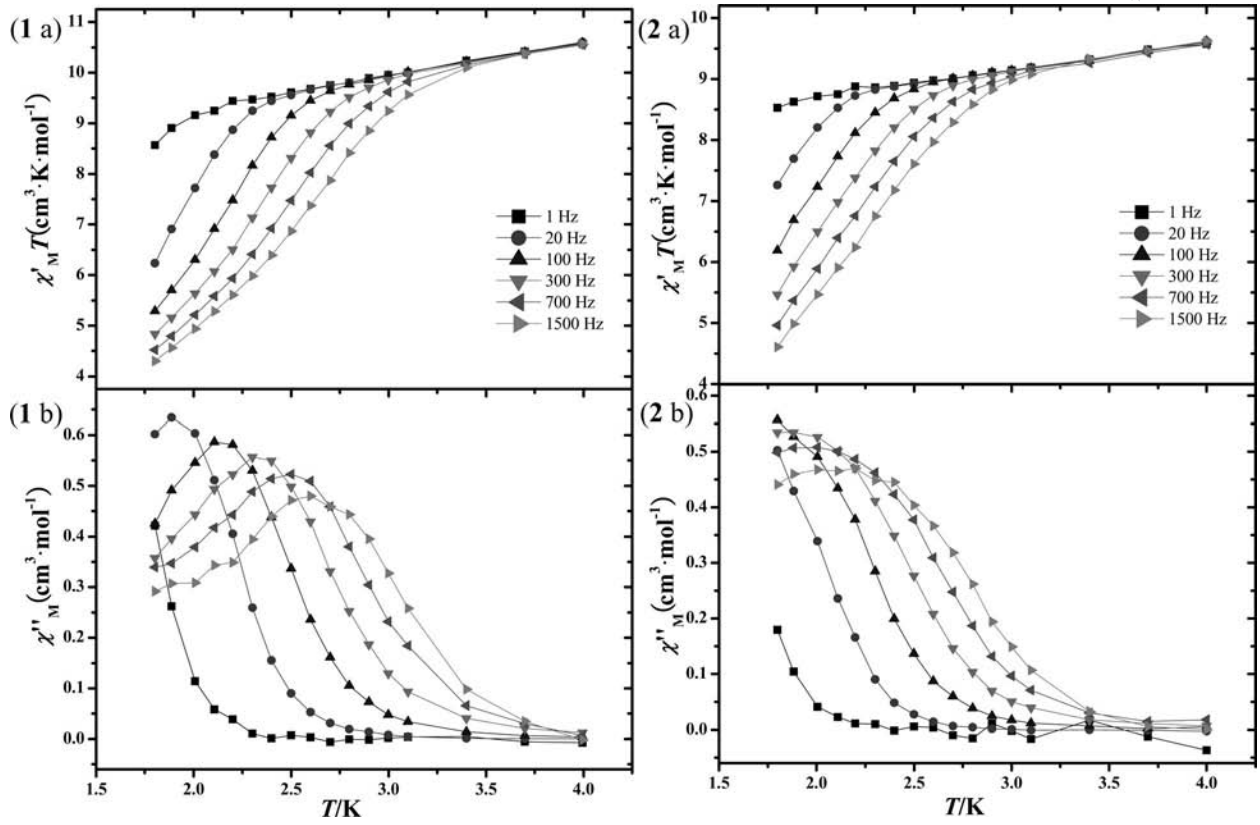


Figure 10. Temperature dependence of the in-phase (**1**a and **2**a for **3** and **4**, respectively) and out-of-phase (**1**b and **2**b for **3** and **4**, respectively) ac susceptibility at the indicated frequencies.

8.4 and 8.1 $cm^3 K mol^{-1}$ for **3** and **4**, respectively, which indicate spin ground state $S = 3$ or 4. Considering the aforementioned fit parameters for **4** and the similarity of the cores of **3** and **4**, we conclude that both **3** and **4** have the same spin ground state $S = 4$.

Because of the presence of $\chi'_M$ peak maximum above 1.8 K in the $\chi'_M$ versus $T$ plots of **3** and **4**, these data can be used to determine the effective kinetic energy barrier ($U_{eff}$) to magnetization relaxation.[16] The data for **3** and **4** are plotted as $\ln(1/\tau)$ versus $1/T$ in Figure 11, and fitted to the Arrhenius equation $\tau = \tau_o \exp(U_{eff}/kT)$, for which $\tau_o$ is the pre-exponential factor, $\tau$ is the relaxation time, and $k$ is the Boltzmann constant. The fit parameters were $U_{eff}$ = 30.0 K and $\tau_o = 1.2 \times 10^{-9}$ s for **3** and $U_{eff}$ = 19.1 K and $\tau_o = 1.3 \times 10^{-8}$ s for **4**. This difference in the effective kinetic energy barrier can be ascribed to the different Jahn–Teller tilts of **3** and **4**. Notably, the effective barrier of **4** is larger than the theoretical upper limit ($U = S^2|D|$) calculated using the $D$ values obtained from the powder dc magnetization measurements (14.5 K). This is expected for exchange-coupled SMMs since the spin reversal is hindered by the relatively weak intermolecular coupling.[7]

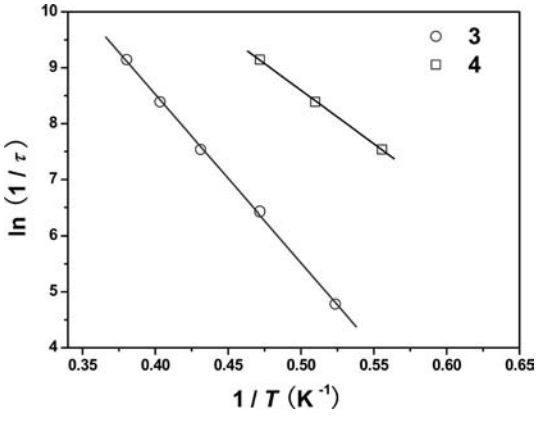


Figure 11. Plots of the natural logarithm of the magnetization relaxation rate versus $1/T$ for complexes **3** (circle) and **4** (square). The solid lines are fits to the Arrhenius equation. See the text for the fit parameters.

## Discussion

The varying magnetic anisotropy of the clusters, which is reflected in $D$ values, is responsible for the significantly different magnetic behavior of the four compounds, especially their ac susceptibility. Accurate evaluation of $D$ requires single-crystal high-frequency EPR (HFEPR) studies,[6] which, in any case, are also complicated by low-lying excited states.[2c] In fact, the $D$ value is consistent with the alignment of four JT axes of the $Mn^{III}$ ions, which are close to co-parallel with small angles (denoted as $\alpha$, it is an approximate gauge of the angle between the JT axes of two $Mn^{III}$ ions).[6,17d] Such arrangement of the JT axes easily leads to a large negative $D$, which has been confirmed by the reported $Mn_2$, $Mn_6$, $Mn_{12}$, $Mn_{21}$, and $Mn_{30}$ SMMs with

  

roughly parallel $Mn^{III}$ JT axes.[3f,17] The angles ($\alpha$) of **1**–**4** are listed in Table 3. It clearly shows that the $\alpha$ of **3** is smaller than the $\alpha$ of **4**. In other words, the JT axes in **3** are more parallel to each other, which leads to a more negative $D$ value, and consequently a higher kinetic-energy barrier. For the same reason, the kinetic-energy barriers of compounds **1** and **2** with larger $\alpha$ than **4** are even smaller. This confirmed the fits of dc magnetization data of **2** and **4**. The small but inescapable difference in the alignment of the four JT axes of the $Mn^{III}$ ions in four compounds is mediated by both intra- and intermolecular interactions. When the $thme^{3-}$ ligands are replaced by $thmp^{3-}$, the pivalate groups in **3** and **4** exhibit different coordinate modes to those in **1** and **2**, thereby inducing more parallel alignments of JT axes. When the terminal aqua ligands in **1** and **3** are replaced by methanol in **2** and **4**, the JT axes arrange in a less parallel conformation to each other. On the other hand, the molecules of **1** and **3**, as well as reported complexes **5**, are involved in extensive hydrogen bonding in the crystal lattice, which introduces very low-lying spin states and leads to the inferior fit of dc magnetization data.

Table 3. The angle ($\alpha$) between the JT axes of two $Mn^{III}$ ions in **1**–**4**.

| | | | |
|---|---|---|---|
| **1** | | | |
| Mn1–Mn2 | 5.2° | | |
| **2** | | | |
| Mn1–Mn2 | 6.0° | | |
| **3** | | | |
| Mn1–Mn7 | 1.4° | Mn2–Mn1 | 3.8° |
| Mn2–Mn7 | 2.5° | Mn2A–Mn2 | 1.8° |
| Mn2A–Mn1 | 3.8° | Mn2A–Mn7 | 2.5° |
| **4** | | | |
| Mn1–Mn2 | 4.4° | | |

Five types of O-bridged $Mn_{12}$ SMMs have been reported so far (Figure 12). Notably, four of them were synthesized by means of Mn carboxylate chemistry. Known as the first and the most widely investigated SMM, $[Mn^{III}_8Mn^{IV}_4O_{12}(O_2CMe)_{16}(H_2O)_4]$ (**6**)[5] possesses an $S$ = 10 spin ground state, $U_{eff}$ = 60 K, and significant magnetic anisotropy ($D$ = –0.5 $cm^{-1}$), on account of a near-parallel alignment of the eight $Mn^{III}$ JT axes, which are roughly perpendicular to the $[Mn_{12}O_{12}]$ disclike core. Furthermore, a family of $Mn_{12}$ SMMs has been reported by means of modifying the original $Mn_{12}$ molecules.[1d] As a contrast, because the alignment of the $Mn^{III}$ JT axes is not parallel, the $D$ values of rodlike $[Mn^{III}_{10}Mn^{II}_2O_4(OH)_2(O_2CPh)_{12}(thme)_4(py)_2]$ (**7**; py = pyridine[4e] ($S$ = 7, $D$ = –0.09 $cm^{-1}$, $U_{eff}$ = 18.3 K) and $[Mn^{III}_9Mn^{II}_3O_7(OH)(OMe)_2(O_2CPh)_{12}(dmhmp)_4(H_2O)]$ (**8**)[3g] ($S$ = 13/2, $D$ = –0.18 $cm^{-1}$, $U_{eff}$ = 11 K) are not so large. Therefore the effective kinetic-energy barriers are not so high. For the $Mn^{III}_xMn^{II}_{12-x}$ ($x$ = 8, 10, and 12)[18] family previously reported by our group, the $Mn^{III}$ ions exhibit rare JT compression, and the fit parameters of $Mn^{III}_{12}$ (**9**) are $S$ = 6 and $D$ = –0.21 $cm^{-1}$. Compared to the above $Mn_{12}$ clusters, the series of valence-sandwich-type $Mn^{III}_4Mn^{II}_8$ in this work do not possesses a large spin ground state ($S$ = 4), but the co-parallel alignment of JT axes of the $Mn^{III}$ ions leads to a large negative $D$ (–0.44 $cm^{-1}$ for **2**, –0.63 $cm^{-1}$ for **4**) even though there are only four $Mn^{III}$ ions in each cluster. On the other hand, the effective kinetic-energy barriers are not very high (30 K for **3**, 19.1 K for **4**) because of the small $S$, but they are still higher than the other $Mn_{12}$ SMMs except the family of $Mn^{III}_8Mn^{IV}_4$.

Substitution of the acetate anion with other carboxylate ligands or oxidization of some of the $Mn^{II}$ ions of the cluster might lead to a larger spin ground state or more negative $D$ values. Studies of this nature are in progress.

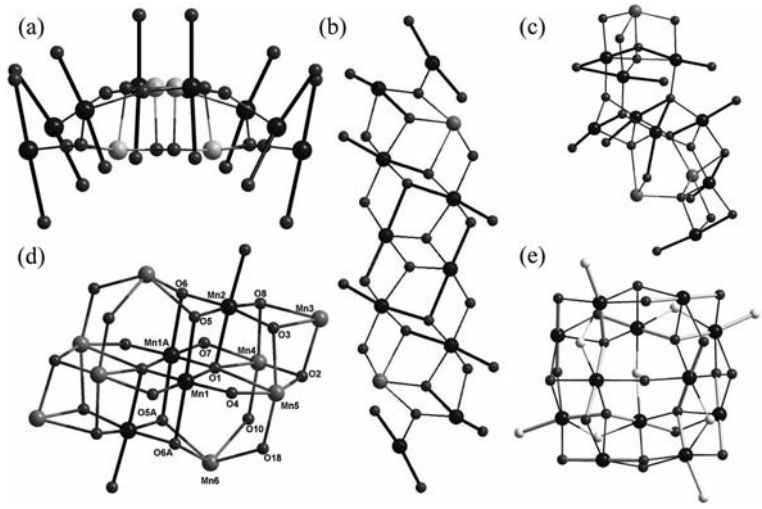


Figure 12. Central core of (a) **6**, (b) **7**, (c) **8**, (d) **3**, (e) **9**. The thicker black bonds indicate the $Mn^{III}$ Jahn–Teller elongation axes. The thicker gray bonds indicate the $Mn^{III}$ Jahn–Teller compression axes.

  

## Conclusion

The use of the tripodal ligands $H_3$thme [1,1,1-tris(hydroxymethyl)ethane] and $H_3$thmp [1,1,1-tris(hydroxymethyl)propane] in Mn carboxylate chemistry has produced a series of valence-sandwich-type $Mn^{III}_4Mn^{II}_8$ clusters, which were all confirmed to be SMMs. More significantly, by substituting tripodal ligands and terminal ligands, the ground-state anisotropy of four $Mn_{12}$ clusters were effectively modified, which may provide a practical way to control the intra- and intermolecular interactions. Further studies are in progress.

## Experimental Section

**General Remarks:** All chemicals were commercially available and used as received without further purification. The C, H, and N microanalyses were carried out with an Elementar Vario-EL CHNS elemental analyzer. The FTIR spectra were recorded from KBr pellets in the range 4000–400 $cm^{-1}$ with a Bio-Rad FTS-7 spectrometer.

**Synthesis of 1:** A mixture of [Mn(acac)$_2$] (0.076 g,0.30 mmol), $H_3$thme (0.012 g, 0.10 mmol), $Me_3CCOOH$(0.020 g, 0.20 mmol), and MeOH/MeCN (v/v 1:1, 15 mL) was sealed in a 25 mL Teflon®-lined, stainless-steel vessel and heated at 120 °C for 50 h, then cooled to room temperature. Red-brown crystals were obtained (yield ca. 49% based on $H_3$thme). $C_{72}H_{136}Mn_{12}O_{38}$ (2269.10): calcd. C 38.11, H 6.04; found C 37.56, H 5.99. Selected IR data (KBr): $\tilde{\nu}$ = 3593 (w), 3436 (m), 2957 (m), 2930 (w), 2869 (w), 1484 (m), 1461 (s), 1384 (m), 1375 (m), 1226 (m), 1121 (m), 1053 (m), 1032 (m), 610 (m), 582 (m) $cm^{-1}$.

**Synthesis of 2:** The procedure was the same as that employed for complex **1**, except that MeOH (15 mL) was employed as solvent instead of mixed MeOH/MeCN. Red-brown crystals were obtained (yield ca. 37% based on $H_3$thme). $C_{74}H_{140}Mn_{12}O_{38}$ (2297.15): calcd. C 38.69, H 6.14; found C 37.96, H 6.01. Selected IR data (KBr): $\tilde{\nu}$ = 3607 (w), 3439 (m), 2955 (m), 2933 (w), 2868 (w), 1486 (m), 1384 (m), 1371 (m), 1225 (m), 1120 (m), 1055 (m), 1036 (m), 608 (m), 581 (m) $cm^{-1}$.

**Synthesis of 3:** The procedure was the same as that employed for complex **1**, except that $H_3$thmp (0.013 g, 0.10 mmol) was employed. Red-brown crystals were again obtained (yield ca. 45% based on $H_3$thmp). $C_{76}H_{144}Mn_{12}O_{38}$ (2325.21): calcd. C 39.26, H 6.24; found C 38.32, H 6.25. Selected IR data (KBr): $\tilde{\nu}$ = 3647 (w), 3626 (w), 3433 (s), 2959 (s), 2907 (m), 2868 (m), 2519 (w), 1634 (w), 1484 (s), 1418 (s), 1384 (s), 1362 (w), 1227 (s), 1112 (s), 1053 (s), 602 (m), 584 (m) $cm^{-1}$.

**Synthesis of 4:** The procedure was the same as that employed for complex **3**, except that MeOH (15 mL) was employed as solvent instead of mixed MeOH/MeCN. Red-brown crystals were again obtained (yield ca. 33% based on $H_3$thmp). $C_{78}H_{148}Mn_{12}O_{38}$ (2353.26): calcd. C 39.81, H 6.34; found C 38.93, H 5.88. Selected IR data (KBr): $\tilde{\nu}$ = 3638 (w), 3429 (m), 2951 (m), 2922 (w), 2872 (w), 1487 (m), 1386 (m), 1368 (m), 1226 (m), 1117 (m), 1052 (m), 604 (m), 584 (m) $cm^{-1}$.

**X-ray Crystallographic Study:** Diffraction intensities were collected with an Oxford Diffraction Gemini R CCD diffractometer with Cu-$K_\alpha$ radiation ($\lambda$ = 1.54056 Å) for **1**–**3** and with a Rigaku R-AXIS SPIDER IP diffractometer with Mo-$K_\alpha$ radiation ($\lambda$ = 0.71073 Å) for **4** at 150(2) K. The raw data frames were integrated with the Bruker SAINT package with a narrow-frame algorithm.[19] Empirical absorption correction based on symmetry-equivalent reflections was applied using the SADABS program. The structures were solved by direct methods, and all non-hydrogen atoms were refined anisotropically by least-squares on $F^2$ using the SHELXTL program.[20] Anisotropic thermal parameters were assigned to all non-hydrogen atoms. The hydrogen atoms attached to carbon were placed in idealized positions and refined using a riding model to the atom to which they were attached. The hydrogen atoms attached to nitrogen and oxygen atoms were experimentally located from the Fourier difference maps and refined with isotropic displacement parameters set to $1.2 \times U_{eq}$ of the attached atoms. Crystal data as well as details of data collection and refinements for complexes are

Table 4. Crystallographic data and structural refinements for **1**–**4**.

| | **1** | **2** | **3** | **4** |
|---|---|---|---|---|
| Formula[a] | $C_{72}H_{136}Mn_{12}O_{38}$ | $C_{74}H_{140}Mn_{12}O_{38}$ | $C_{76}H_{144}Mn_{12}O_{38}$ | $C_{78}H_{148}Mn_{12}O_{38}$ |
| $M_r$[a] | 2269.09 | 2297.14 | 2325.19 | 2353.24 |
| $T$ [K] | 150(2) | 150(2) | 150(2) | 150(2) |
| Crystal color and form | brown block | brown needle | brown block | brown block |
| Crystal system | triclinic | monoclinic | orthorhombic | monoclinic |
| Space group | $P\bar{1}$ | $C2/c$ | $Pccn$ | $C2/c$ |
| $a$ [Å] | 12.7485(5) | 25.8363(9) | 26.4332(7) | 27.319(1) |
| $b$ [Å] | 14.9422(5) | 16.4266(3) | 15.1897(4) | 16.393(1) |
| $c$ [Å] | 15.0737(4) | 24.0997(8) | 24.6284(7) | 24.115(1) |
| $\alpha$ [°] | 118.122(3) | 90 | 90 | 90 |
| $\beta$ [°] | 103.753(3) | 104.735(3) | 90 | 108.093(6) |
| $\gamma$ [°] | 96.057(3) | 90 | 90 | 90 |
| $V$ [Å$^3$] | 2379.1(1) | 9891.6(5) | 9888.6(5) | 10266(1) |
| $Z$ | 1 | 4 | 4 | 4 |
| $D_{calcd.}$ [g cm$^{-3}$] | 1.584 | 1.543 | 1.562 | 1.523 |
| $\mu$ [mm$^{-1}$] | 13.169 | 12.677 | 12.688 | 1.499 |
| Reflections collected/unique | 13285/7020 | 14253/7693 | 13093/ | 14316/8005 |
| Parameters | 568 | 578 | 586 | 596 |
| GOF | 0.970 | 0.961 | 0.975 | 0.922 |
| $R_1$ [$I \geq 2\sigma(I)$][b,c] | 0.0486 | 0.0633 | 0.0901 | 0.0663 |
| $wR_2$ (all data)[b,c] | 0.1232 | 0.1965 | 0.2338 | 0.1674 |
| Residues [e Å$^{-3}$] | 0.619/–0.853 | 1.514/–1.022 | 1.253/–0.605 | 1.056/–0.683 |

[a] Including solvate molecules. [b] $R_1 = \Sigma||F_o| - |F_c||/\Sigma|F_o|$. [c] $wR_2 = [\Sigma w(F_o^2 - F_c^2)^2/\Sigma w(F_o^2)^2]^{1/2}$.

  

summarized in Table 4. Selected bond lengths and angles are listed in Table S1 in the Supporting Information The ORTEP plots and packing pictures were produced with Diamond 3.1.[21]

CCDC-809668 (for **1**), -809669 (for **2**), -809670 (for **3**) and 809671 (for **4**) contain the supplementary crystallographic data for this paper. These data can be obtained free of charge from The Cambridge Crystallographic Data Centre via www.ccdc.cam.ac.uk/data_request/cif.

**Supporting Information** (see footnote on the first page of this article): Central cores of **2**–**4**, plots of *M* versus *H* of **1**–**4** at 1.8 K, selected bonds and angles in **1**–**4**, and BVS for selected O atoms in **1**–**4** are presented.

## Acknowledgments

This work was supported by the National Natural Science Foundation of China (NSFC) (grant numbers 20525102, 20821001, 90922009, and 50872157) and the National Basic Research Program of China (973 Program, Grant 2007CB815305).

[1] For reviews, see: a) G. Christou, D. Gatteschi, D. N. Hendrickson, R. Sessoli, *MRS Bull.* **2000**, *25*, 66–71; b) D. Gatteschi, R. Sessoli, *Angew. Chem. Int. Ed.* **2003**, *43*, 268–297; c) G. Aromí, E. K. Brechin, *Struct. Bonding (Berlin)* **2006**, *122*, 1–67; d) R. Bagai, G. Christou, *Chem. Soc. Rev.* **2009**, *38*, 1011–1026.

[2] a) J. R. Friedman, M. P. Sarachik, J. Tejada, R. Ziolo, *Phys. Rev. Lett.* **1996**, *76*, 3830; b) L. Thomas, L. Lionti, R. Ballou, D. Gatteschi, R. Sessoli, B. Barbara, *Nature* **1996**, *383*, 145; c) S. Hill, S. Datta, J. Liu, R. Inglis, C. J. Milios, P. L. Feng, J. J. Henderson, E. del Barco, E. K. Brechin, D. N. Hendrickson, *Dalton Trans.* **2010**, *39*, 4693–4707.

[3] a) M. W. Wemple, H.-L. Tsai, K. Folting, D. N. Hendrickson, G. Christou, *Inorg. Chem.* **1993**, *32*, 2025–2031; b) P. King, W. Wernsdorfer, K. A. Abboud, G. Christou, *Inorg. Chem.* **2004**, *43*, 7315–7323; c) M. Murugesu, M. Habrych, W. Wernsdorfer, K. A. Abboud, G. Christou, *J. Am. Chem. Soc.* **2004**, *126*, 4766–4767; d) M. Soler, W. Wernsdorfer, K. Folting, M. Pink, G. Christou, *J. Am. Chem. Soc.* **2004**, *126*, 2156–2165; e) A. J. Tasiopoulos, A. Vinslava, W. Wernsdorfer, K. A. Abboud, G. Christou, *Angew. Chem. Int. Ed.* **2004**, *43*, 2117–2121; f) C. Lampropoulos, G. Redler, S. Data, K. A. Abboud, S. Hill, G. Christou, *Inorg. Chem.* **2010**, *49*, 1325–1336; g) T. Taguchi, W. Wernsdorfer, K. A. Abboud, G. Christou, *Inorg. Chem.* **2010**, *49*, 199–208; h) E. Cremades, J. Cano, E. Ruiz, G. Rajaraman, C. J. Milios, E. K. Brechin, *Inorg. Chem.* **2009**, *48*, 8012–8019; i) W.-G. Wang, A.-J. Zhou, W.-X. Zhang, M.-L. Tong, X.-M. Chen, M. Nakano, C. C. Beedle, D. N. Hendrickson, *J. Am. Chem. Soc.* **2007**, *129*, 1014–1015; j) A.-J. Zhou, J.-L. Liu, R. Herchel, J.-D. Leng, M.-L. Tong, *Dalton Trans.* **2009**, 3182–3192; k) J.-L. Liu, J.-D. Leng, M.-L. Tong, *Chem. Asian. J.* **2011**, *6*, 1007–1010

[4] a) A. Mishra, W. Wernsdorfer, S. Parsons, G. Christou, E. K. Brechin, *Chem. Commun.* **2005**, 2086–2088; b) R. T. W. Scott, S. Parsons, M. Murugesu, W. Wernsdorfer, G. Christou, E. K. Brechin, *Chem. Commun.* **2005**, 2083–2085; c) C.-M. Liu, D.-Q. Zhang, D.-B. Zhu, *Inorg. Chem.* **2009**, *48*, 792–794; d) G. Rajaraman, M. Murugesu, E. C. Sanudo, M. Soler, W. Wernsdorfer, M. Helliwell, C. Muryn, J. Raftery, S. J. Teat, G. Christou, E. K. Brechin, *J. Am. Chem. Soc.* **2004**, *126*, 15445–15457; e) E. K. Brechin, M. Soler, G. Christou, M. Helliwell, S. J. Teat, W. Wernsdorfer, *Chem. Commun.* **2003**, 1276–1277; f) E. K. Brechin, M. Soler, J. Davidson, D. N. Hendrickson, S. Parsons, G. Christou, *Chem. Commun.* **2002**, 2252–2253; g) Y.-G. Li, W. Wernsdorfer, R. Clérac, I. J. Hewitt, C. E. Anson, A. K. Powell, *Inorg. Chem.* **2006**, *45*, 2376–2378; h) M. Murugesu, W. Wernsdorfer, K. A. Abboud, E. K. Brechin, G. Christou, *Dalton Trans.* **2006**, 2285–2287; i) M. Murugesu, J. Raftery, W. Wernsdorfer, G. Christou, E. K. Brechin, *Inorg. Chem.* **2004**, *43*, 4203–4209.

[5] a) R. Sessoli, D. Gatteschi, A. Caneschi, M. A. Novak, *Nature* **1993**, *365*, 141; b) R. Sessoli, H.-L. Tsai, A. R. Schake, S. Wang, J. B. Vincent, K. Folting, D. Gatteschi, G. Christou, D. N. Hendrickson, *J. Am. Chem. Soc.* **1993**, *115*, 1804.

[6] a) D. Gatteschi, L. Sorace, *J. Solid State Chem.* **2001**, *159*, 253–261; b) H. Oshio, M. Nakano, *Chem. Eur. J.* **2005**, *11*, 5178–5185; c) A. Bencini, D. Gatteschi, *EPR of Exchange Coupled Systems*, Springer, Berlin, Germany, **1990**.

[7] R. Inglis, S. M. Taylor, L. F. Jones, G. S. Papaefstathiou, S. P. Perlepes, S. Datta, S. Hill, W. Wernsdorfer, E. K. Brechin, *Dalton Trans.* **2009**, 9157–9168.

[8] a) M. I. Khan, J. Zubieta, *Prog. Inorg. Chem.* **1995**, *43*, 1–149; b) M. Cavaluzzo, Q. Chen, J. Zubieta, *J. Chem. Soc., Chem. Commun.* **1993**, 131–132; c) R. C. Finn, J. Zubieta, *J. Cluster Sci.* **2000**, *11*, 461–482; d) R. W. Saalfrank, I. Bernt, E. Uller, F. Hampel, *Angew. Chem. Int. Ed. Engl.* **1997**, *36*, 2482–2485.

[9] a) L. F. Jones, A. Batsanov, E. K. Brechin, D. Collison, M. Helliwell, T. Mallah, E. J. L. McInnes, S. Piligkos, *Angew. Chem. Int. Ed.* **2002**, *41*, 4318–4321; b) M. Moragues-Canovas, M. Helliwell, L. Ricard, É. Rivière, W. Wernsdorfer, E. K. Brechin, T. Mallah, *Eur. J. Inorg. Chem.* **2004**, 2219–2212; c) E. K. Brechin, *Chem. Commun.* **2005**, 5141–5153.

[10] For a minireview, see: R. Laye, E. J. L. McInnes, *Eur. J. Inorg. Chem.* **2004**, 2811–2818.

[11] A. Rabenau, *Angew. Chem. Int. Ed. Engl.* **1985**, *24*, 1026–1040.

[12] a) I. D. Brown, D. Altermatt, *Acta Crystallogr., Sect. B* **1985**, *41*, 244–247; b) W. Liu, H. H. Thorp, *Inorg. Chem.* **1993**, *32*, 4102–4105.

[13] M. Affronte, J. C. Lasjounias, W. Wernsdorfer, R. Sessoli, D. Gatesschi, S. L. Heath, A. Fort, A. Rettori, *Phys. Rev. B: Condens. Matter* **2002**, *66*, 064408/1–064408/7.

[14] This program assumes that only the ground states are populated, including $D_m$, $E_m$, *g*, and Zeeman interactions, and incorporating a full powder average; for details, see M. P. Shores, J. J. Sokol, J. R. Long, *J. Am. Chem. Soc.* **2002**, *124*, 2279–2292.

[15] P. King, W. Wernsdorfer, K. A. Abboud, G. Christou, *Inorg. Chem.* **2005**, *44*, 8659.

[16] M. A. Novak, R. Sessoli, in: *Quantum Tunneling of Magnetization - QTM '94*, (Eds.: L. Gunther, B. Barbara), Kluwer, Amsterdam, **1995**, pp. 171–188.

[17] a) L. S. Kramer, A. W. Clauss, L. C. Francesconi, D. R. Corbin, D. N. Hendrickson, G. D. Stucky, *Inorg. Chem.* **1981**, *20*, 2070–2077; b) Y.-Z. Zheng, M.-L. Tong, W.-X. Zhang, X.-M. Chen, *Angew. Chem. Int. Ed.* **2006**, *45*, 6310–6314; c) Y.-Z. Zheng, M.-L. Tong, W.-X. Zhang, X.-M. Chen, *Chem. Commun.* **2006**, 165–167; d) Y.-Z. Zheng, W. Xue, W.-X. Zhang, M.-L. Tong, X.-M. Chen, *Inorg. Chem.* **2007**, *46*, 6437–6443.

[18] A.-J. Zhou, L.-J. Qin, C. C. Beedle, S. Ding, M. Nakano, J.-D. Leng, M.-L. Tong, D. N. Hendrickson, *Inorg. Chem.* **2007**, *46*, 8111–8113.

[19] R. H. Blessing, *Acta Crystallogr., Sect. A* **1995**, *51*, 33.

[20] *SHELXTL 6.10*, Bruker Analytical Instrumentation, Madison, WI, **2000**.

[21] W. T. Pennington, *J. Appl. Crystallogr.* **1999**, *32*, 1028–1029.

Received: January 27, 2011
Published Online: April 1, 2011

  